Velocity slip in microscale cylindrical Couette flow: The Langmuir model

R. S. Myong
Department of Mechanical Engineering, University of Strathclyde, Glasgow G1 1XJ, United Kingdom and Department of Mechanical and Aerospace Engineering, Gyeongsang National University, Chinju, Kyeongnam 660-701, South Korea

J. M. Reese
Department of Mechanical Engineering, University of Strathclyde, Glasgow G1 1XJ, United Kingdom

R. W. Barber and D. R. Emerson
Centre for Microfluidics and Microsystems Modelling, Council for the Central Laboratory of the Research Councils (CCLRC) Daresbury Laboratory, Warrington WA4 4AD, United Kingdom

(Received 30 December 2004; accepted 20 June 2005; published online 9 August 2005)

The velocity slip on the solid surfaces of microscale cylindrical Couette flow is investigated using the Langmuir adsorption model for the gas-surface molecular interaction. The accommodation coefficient in the Maxwell model, which is a free parameter based on the concept of diffusive reflection, is replaced by a physical parameter of heat adsorption in the Langmuir model. The phenomenon of velocity inversion is then clearly explained by introducing a velocity polar on the hodograph plane. It is also shown that the quantity used to determine the momentum slip in a concentric cylindrical geometry should be based upon the angular velocity, not the velocity itself. Finally, and despite their totally independent considerations of the gas-surface molecular interaction, the Maxwell and Langmuir slip models are shown to be in qualitative agreement with direct simulation Monte Carlo data in capturing the general features of the flow field. © *2005 American Institute of Physics*. [DOI: 10.1063/1.2003154]

I. INTRODUCTION

Recently there has been renewed interest in understanding the fundamental physics of gas transport phenomena in micro- and nanodevices.[1,2] This is largely driven by the need for new theoretical tools to accurately model microscale physical processes and to design devices with enhanced performance. The mathematical difficulties associated with the hypersonic rarefied flow regimes do not appear in microfluidics because of the relatively low flow speeds. Instead, the physics at solid surfaces play a critical role in microfluidic transport since the relative importance of surface forces increases as the device size shrinks to the microscale. One of these prominent surface forces is the van der Waals force in the interaction of gas molecules and surface atoms.

Modeling the molecular interaction between gas particles and the solid-surface atoms is accomplished by a boundary condition in any theoretical or computational approach. The problem of defining such a boundary condition involves, in general, the kinetic theory of gases[3–6] and solid-state physics. In principle, one could modify the Boltzmann equation to include gas-surface interactions, but the difficulty in developing such a theory has meant that most previous works have been based on the scattering kernel. A kernel with two parameters, known as the Cercignani-Lampis model,[7] and the reduction of the kernel to the accommodation coefficient in Maxwell's model[8] have been used extensively.

The effect of gas-surface interaction on microfluidic transport has been studied in recent experimental work on microchannels.[9,10] This confirmed that conventional theories are unable to predict important flow features, for example, the increase in the mass flow rate. Moreover, this work also demonstrated that such discrepancies can be resolved by incorporating surface effects using the aforementioned slip models. There are also several studies[11–18] which have attempted to extend the slip models—originally applicable only to planar surfaces—to flows over curved surfaces as well. The effect of the boundary curvature radius on the slip length was investigated by Einzel, Panzer, and Liu,[14] who developed a general hydrodynamic boundary condition on curved surfaces. By analyzing the cylindrical Couette flow with a rotating inner cylinder and a stationary outer cylinder, they demonstrated that the velocity slip can cause the expected velocity profile across the radius to become inverted (i.e., the tangential velocity increases with distance from the rotating inner cylinder). This anomalous velocity profile, which was initially considered physically unrealistic,[19] has been called "velocity inversion" in the literature. Tibbs, Baras, and Garcia[15] also investigated the effect of curvature on the slip length by performing direct simulation Monte Carlo[20] (DSMC) calculations of the motion of hard-sphere particles in microscale cylindrical Couette flow. They found that the values of the accommodation coefficients in the slip model have a large impact on the phenomenon of velocity inversion, and their analytical results were in qualitative agreement with the DSMC data. A similar study by Aoki, Yoshida, Nakanishi, and Garcia,[16] using a numerical solution of the Boltzmann equation with the Bhatnagar-Gross-Krook (BGK) approximation and the DSMC method, again confirmed the existence of the velocity-inversion phenomenon in the case of large velocity slip at the cylinders. Recent studies

by Lockerby, Reese, Emerson, and Barber[17] and Yuhong, Barber, and Emerson[18] investigated the velocity-inversion process in cylindrical Couette flow using the original Maxwell model which depends on the shear stress rather than the tangential velocity gradient. The influence of different accommodation coefficients at the inner and outer walls was explored and the existence of a common point through which the family of velocity profiles all pass was demonstrated.

Nonetheless, there exists a room for improvement in these models because the concept of an accommodation coefficient does not incorporate the variation of slip coefficient (or accommodation coefficient) with the type of gas or the nature of the wall material. Recently, some works[21–25] have attempted to attribute physical meaning to the accommodation coefficient from the viewpoint of adsorption—a well-developed field in the physical chemistry of surfaces.[26,27] In this approach the gas molecules are assumed to interact with the surface of the solid via a long-range force; consequently, the gas molecules can be adsorbed onto the surface and then desorbed after some time lag. The fraction of adsorbed molecules in this process can be determined by an adsorption isotherm, for example, the famous Langmuir isotherm. Therefore, it is possible to develop a simple slip model, based on the gas-surface interaction, where information on the shear stress or velocity gradient at the wall is not required. This method, called "the Langmuir slip model," has been successfully applied to several flow problems of interest: planar Couette flow,[21,22] pressure-driven microchannel flow, and low Reynolds number flow past a sphere.[23,24] It has been shown that this Langmuir model recovers the Maxwell model in its first-order approximation and therefore a physical meaning can now be assigned to the slip coefficient in the Maxwell model.[24]

In the present paper we use this new slip model of the gas-surface molecular interaction to investigate theoretically the velocity slip in microscale cylindrical Couette flow. The emphasis is on the effects of curvature and nonequilibrium on the general flow field. We demonstrate that, in spite of their totally independent considerations of the gas-surface interaction, both models are in qualitative agreement with each other in capturing the general features of the flow field, including the velocity-inversion phenomenon. Moreover, in the course of the investigation we introduce a velocity polar to describe concisely the flow topology: all the information on the velocity profiles (noninverted, partially inverted, or fully inverted) are easily identified on this polar.

II. ROTATING CYLINDRICAL COUETTE FLOW

We consider the isothermal Couette flow between two microscale concentric rotating cylinders. The Navier-Stokes equations with constant properties reduce to the following form under these special assumptions and geometry:[11,12]

$$\frac{1}{r^2}\frac{d}{dr}(r^2\tau_{r\theta})=0 \quad \text{where} \quad \tau_{r\theta}=\mu\left[r\frac{d}{dr}\left(\frac{u_\theta}{r}\right)\right]. \tag{1}$$

The tangential velocity u_θ is assumed to be a function of the radial coordinate r only, satisfying the continuity equation automatically; μ denotes the Chapman-Enskog viscosity. Even though Eq. (1) is valid for compressible flow, the present study will be restricted to incompressible flow. The general solution of Eq. (1) can be written as

$$u_\theta(r)=ar+br^{-1}, \tag{2}$$

where the coefficients a and b will be determined by the boundary conditions. For this velocity profile, the shear stress $\tau_{r\theta}$ reduces to

$$\tau_{r\theta}=-2\mu br^{-2}. \tag{3}$$

If we consider the flow defined by the inner and outer cylinders with radii R_1 and R_2, then the boundary conditions become

$$u_{\theta_1}=aR_1+bR_1^{-1}, \quad u_{\theta_2}=aR_2+bR_2^{-1}, \tag{4}$$

where u_{θ_1} and u_{θ_2} represent the velocity at $r=R_1$ and $r=R_2$, respectively. Then the coefficients a and b can be expressed in terms of the gas velocities on the cylinders

$$a=\frac{1}{D}\left(\frac{u_{\theta_1}}{R_2}-\frac{u_{\theta_2}}{R_1}\right), \quad b=\frac{1}{D}(u_{\theta_2}R_1-u_{\theta_1}R_2),$$

where

$$D=\chi-\chi^{-1} \quad \text{and} \quad \chi\equiv\frac{R_1}{R_2}(<1). \tag{5}$$

We use the solutions of the form given in Eq. (2), with coefficients a and b, to investigate the general features of the flow field, as it turns out that the topology of the flow field is best represented in terms of the velocities u_{θ_1} and u_{θ_2}. The conventional form of the solutions are, however, expressed in terms of the angular velocities of the cylinders, Ω_1 and Ω_2.

Following the notation adopted by Einzel, Panzer, and Liu,[14] the solution (2) can be put into another form

$$u_\theta(r)=\frac{A\Omega_1-B\Omega_2}{A-B}r+\frac{\Omega_1-\Omega_2}{B-A}r^{-1}, \tag{6}$$

where

$$A=\frac{1}{b}(\Omega_2-a)=\frac{1}{R_2^2}\left[\frac{DR_2\Omega_2+\chi^{-1}u_{\theta_2}-u_{\theta_1}}{\chi u_{\theta_2}-u_{\theta_1}}\right]$$

and

$$B=\frac{1}{b}(\Omega_1-a)=\frac{1}{R_1^2}\left[\frac{DR_1\Omega_1+u_{\theta_2}-\chi u_{\theta_1}}{u_{\theta_2}-\chi^{-1}u_{\theta_1}}\right]. \tag{7}$$

Then the derivatives of velocity in the radial direction can be written as

$$\frac{du_\theta}{dr}=\frac{1}{(A-B)}[A\Omega_1-B\Omega_2+(\Omega_1-\Omega_2)r^{-2}], \tag{8}$$

where

$$A - B = -\frac{1}{b}(\Omega_1 - \Omega_2).$$

The sign of Eq. (8) provides information on the increase or decrease of the velocity in the radial direction. For example, if $\Omega_2 = 0$, a positive sign requires

$$A - B < 0 \text{ and } A + r^{-2} < 0 \text{ (equivalently } A + R_1^{-2} < 0).$$

This condition can be rewritten in terms of a and b,

$$0 < b < aR_1^2.$$

If we assume u_{θ_1} and u_{θ_2} to be nonnegative, then it reduces to

$$\chi < \frac{u_{\theta_1}}{u_{\theta_2}} < \frac{2\chi}{1+\chi^2}. \tag{9}$$

A. Langmuir slip model

A physical approach to describing the slip can be developed by taking into account the interfacial interaction between the gas molecules and the surface (which itself consists of molecules). In this approach the gas molecules are assumed to interact with the surface of the solid via a long-range force, and consequently the gas molecules can be adsorbed onto the surface and then desorbed after some time lag. This mechanism of deposition of a layer with a thickness of one or more molecules onto the surface is known as adsorption in the literature of surface chemistry.[26,27] If we model this interaction as a chemical reaction in which the gas molecule m and the site s form the complex c, we may obtain an expression for the fraction of the surface covered by adsorbed atoms at thermal equilibrium, α,[21] as

$$\alpha = (1-\alpha)\beta p \quad \text{or} \quad \alpha = \frac{\beta p}{1+\beta p},$$

where

$$\beta = \frac{K}{k_B T_w} \quad \text{and} \quad K = \frac{C_c}{C_m C_s}. \tag{10}$$

This fraction α is a function of the pressure p and the equilibrium constant K, which are functions of the concentration $C_{m,s,c}$ and the surface temperature T_w. As the pressure increases, α approaches unity, implying that most of the molecules are at thermal equilibrium.

Using this Langmuir adsorption isotherm (10), it is possible to develop a slip model for the gas-surface molecular interaction. The gas velocity at the wall can be expressed, in dimensional form, as[21,23,24]

$$u = \alpha u_w + (1-\alpha)u_g, \tag{11}$$

where the subscript g denotes the local value adjacent to the wall, for example, a mean free path away from the wall, or a reference value such as the free-stream condition. In a previous study[24] it was shown that the parameter α in the incompressible limit takes the following form:

$$\alpha = \frac{\bar{\beta}}{1+\bar{\beta}} \quad \text{where} \quad \bar{\beta} = \frac{1}{4\omega \mathrm{Kn}}, \tag{12}$$

where Kn is the Knudsen number. So, in other words,

$$\alpha = \frac{1}{1+4\omega \mathrm{Kn}}. \tag{13}$$

In these equations the following definition has been used:

$$\omega = \omega_0(\nu)\left(\frac{T_w}{T_r}\right)^{1+2/(\nu-1)} \exp\left(-\frac{D_e}{k_B T_w}\right), \tag{14}$$

where

$$\omega_0(\nu) = \frac{8\sqrt{2}}{5\pi} A_2(\nu)\Gamma[4 - 2/(\nu-1)]. \tag{15}$$

Here ν is the exponent of the inverse power law for the particle interaction potential and $A_2(\nu)$ is a pure number available in monographs on kinetic theory.[3,6] The value of ω_0 lies between 1.02806 (for $\nu=6$) and 1.52001 (for $\nu=3$), and becomes 1.44051 (for $\nu \to \infty$) in the case of rigid elastic spheres. In this model the slip coefficient ω varies with the type of gas via ν and with the nature of the wall material via the potential energy of heat adsorption D_e. In fact, the role of the coefficient ω, which is also a function of the wall temperature T_w, is very similar to the slip coefficient ω_M of the Maxwell model. In the Maxwell model, the slip coefficient ω_M is related to the accommodation coefficient σ by

$$\omega_M = \frac{2-\sigma}{\sigma}. \tag{16}$$

It should be noted here that the slip coefficient ω in the Langmuir model is a physical parameter of heat adsorption while the accommodation coefficient σ in the Maxwell model is a free parameter based on the concept of diffusive reflection.

For the cylindrical Couette flow with inner and outer cylinders rotating at angular velocities Ω_1 and Ω_2, the gas velocities on the cylinders in the Langmuir slip model may be expressed as

$$u_{\theta_1} = \alpha_1 R_1 \Omega_1 + (1-\alpha_1)u_\theta(\bar{R})\frac{R_1}{\bar{R}}, \tag{17}$$

$$u_{\theta_2} = \alpha_2 R_2 \Omega_2 + (1-\alpha_2)u_\theta(\bar{R})\frac{R_2}{\bar{R}}. \tag{18}$$

The Knudsen number in the present problem is defined as

$$\mathrm{Kn} = \frac{\lambda}{R_2 - R_1},$$

where λ denotes the gas molecular mean free path. It should be noted that using the same λ for the equations at the inner and outer cylinders means that the radial gradient of the density profile is neglected in the present formulation. $\bar{R}$ represents the radius of the reference position, which becomes an average of the radii of the inner and outer cylinders when $R_1 \approx R_2$. Otherwise it varies, depending on the radius of cur-

vature at the wall. It should be noted that the ratio terms $R_1/\bar{R}$ and $R_2/\bar{R}$ appear in these equations. Their origin can be traced to the extended version of the Langmuir slip model in concentric rotating cylinders:

$$\Omega = \alpha\Omega_w + (1-\alpha)\Omega_g. \tag{19}$$

For further analysis, the following dimensionless quantities are introduced for the case of a stationary outer cylinder:

$$u_\theta^* \equiv \frac{u_\theta}{R_1\Omega_1}, \quad \bar{\Omega} \equiv \frac{\Omega_2}{\Omega_1}, \quad r^* \equiv \frac{r}{R_1}, \quad \bar{R}^* \equiv \frac{\bar{R}}{R_1}$$

and

$$1 \leqslant r^* \leqslant \chi^{-1}.$$

If we restrict our interest to the simplest case with $\alpha_1=\alpha_2(=\alpha)$ and $\Omega_2=0$, then the solutions can be written as

$$u_{\theta_1}^* = 1-(1-\alpha)\frac{1}{1+\chi^3}, \tag{20}$$

$$u_{\theta_2}^* = (1-\alpha)\frac{\chi^2}{1+\chi^3}. \tag{21}$$

The corresponding velocity profile reduces to

$$u_\theta^*(r^*) = \frac{a}{\Omega_1}r^* + \frac{b}{R_1^2\Omega_1}r^{*-1}, \tag{22}$$

where

$$a = \frac{\Omega_1}{D}\chi\left[1-\frac{1-\alpha}{1-\chi+\chi^2}\right] \quad \text{and} \quad b = -\frac{R_1^2\Omega_1}{D}\frac{\alpha}{\chi}.$$

(For details, see Appendix A.) In the conventional notation of Eqs. (7), we have

$$A = \frac{1}{R_2^2}\left[1-\chi\frac{(1-\alpha)(1-\chi)}{\alpha(1-\chi+\chi^2)}\right]$$

and

$$B = \frac{1}{R_1^2}\left[1+\frac{(1-\alpha)(1-\chi)}{\alpha(1-\chi+\chi^2)}\right].$$

In the limit $\alpha\to 1$, the following continuum solutions are then recovered:

$$u_\theta^*(r^*) = \frac{1}{D}\left[\chi r^* - \frac{1}{\chi}r^{*-1}\right] \quad \text{and} \quad u_{\theta_1}^* = 1, \quad u_{\theta_2}^* = 0.$$

In the limit $\alpha\to 0$, the solution is a solid-body rotation,

$$u_\theta^*(r^*) = \frac{\chi^3}{1+\chi^3}r^* \quad \text{and} \quad u_{\theta_1}^* = \frac{\chi^3}{1+\chi^3}, \quad u_{\theta_2}^* = \frac{\chi^2}{1+\chi^3}.$$

In addition, the shear stresses on the cylinders are

$$\left[\frac{\tau_{r\theta}}{\mu\Omega_1}\right]_{r^*=1} = \chi^{-2}\left[\frac{\tau_{r\theta}}{\mu\Omega_1}\right]_{r^*=1/\chi} = -\frac{2\alpha}{1-\chi^2},$$

from

$$\frac{\tau_{r\theta}}{\mu\Omega_1} = -\frac{2b}{R_1^2\Omega_1}r^{*-2}.$$

With the velocity profile determined, the mechanical pressure distribution can be obtained by integrating the radial momentum equation:

$$p^*(r^*) = p_1^* + \frac{1}{2}\left(\frac{a}{\Omega_1}\right)^2(r^{*2}-1) - \frac{1}{2}\left(\frac{b}{R_1^2\Omega_1}\right)^2(r^{*-2}-1) + \frac{2ab}{R_1^2\Omega_1^2}\ln r^*,$$

where

$$p^* = \frac{p}{\rho(R_1\Omega_1)^2}.$$

B. Maxwell slip model

An alternative way of incorporating the slip is to make a correction based on the degree of nonequilibrium near the wall surface which can best be represented via the shear stress. This idea can be traced to the work of Maxwell[8] in which the following slip velocity boundary condition is proposed:

$$u_\theta = u_{\theta_w} + \varsigma\tau_{r\theta_w} = u_{\theta_w} + \frac{\omega_M}{\mu}\lambda\left[\mu r\frac{d}{dr}\left(\frac{u_\theta}{r}\right)\right]_w, \quad \text{where} \quad \omega_M = \frac{2-\sigma}{\sigma}, \tag{23}$$

where u_θ, $\tau_{r\theta_w}$, and ς represent the velocity, the shear stress at the wall, and the slip length divided by the viscosity, respectively. (The constitutive equation for the shear stress is treated as linear here.) The values of the accommodation coefficient σ are usually chosen to fit the experimental data, and are tabulated for various gases and surfaces.

The Maxwell slip model can be written in cylindrical form as follows:

$$u_{\theta_1} = R_1\Omega_1 + \omega_{M_1}\lambda\left[r\frac{d}{dr}\left(\frac{u_\theta}{r}\right)\right]_{r=R_1}, \tag{24}$$

$$u_{\theta_2} = R_2\Omega_2 - \omega_{M_2}\lambda\left[r\frac{d}{dr}\left(\frac{u_\theta}{r}\right)\right]_{r=R_2}. \tag{25}$$

After introducing the definition

$$\alpha_M = \frac{1}{1+4\omega_M\mathrm{Kn}},$$

and applying Eq. (3), we obtain the following solutions $[\alpha_{M_1}=\alpha_{M_2}(=\alpha_M),\Omega_2=0]$:

$$u_{\theta_1}^* = \frac{2\alpha_M\chi(1+\chi)+(1-\alpha_M)\chi^3}{2\alpha_M\chi(1+\chi)+(1-\alpha_M)(1+\chi^3)}, \tag{26}$$

$$u_{\theta_2}^* = \frac{(1-\alpha_M)\chi^2}{2\alpha_M\chi(1+\chi)+(1-\alpha_M)(1+\chi^3)}. \tag{27}$$

In terms of our notation a, b and A, B, we have

$$a = \frac{\Omega_1}{D}\left[\frac{\chi^2(1+\chi)[2\alpha_M-(1-\alpha_M)(1-\chi)]}{2\alpha_M\chi(1+\chi)+(1-\alpha_M)(1+\chi^3)}\right]$$

and

$$b = -\frac{R_1^2\Omega_1}{D}\left[\frac{2\alpha_M(1+\chi)}{2\alpha_M\chi(1+\chi)+(1-\alpha_M)(1+\chi^3)}\right],$$

$$A = \frac{1}{R_2^2}\left[1-\frac{(1-\alpha_M)}{2\alpha_M}(1-\chi)\right]$$

and

$$B = \frac{1}{R_1^2}\left[1+\frac{(1-\alpha_M)}{2\alpha_M}(1-\chi)\right].$$

(For details, see Appendix B. The earlier derivation of the solutions of the Maxwell slip model can be found in Refs. 11 and 12.)

Analogous to the Langmuir model, these solutions reduce to the continuum solution when $\alpha_M \to 1$. It also turns out that the solution in the limit $\alpha_M \to 0$ is exactly the same as in the Langmuir model. In addition, the shear stresses on the cylinders in the Maxwell model can be written as

$$\left[\frac{\tau_{r\theta}}{\mu\Omega_1}\right]_{r^*=1} = \chi^{-2}\left[\frac{\tau_{r\theta}}{\mu\Omega_1}\right]_{r^*=1/\chi} = \frac{-4\alpha_M\chi}{(1-\chi)[2\alpha_M\chi(1+\chi)+(1-\alpha_M)(1+\chi^3)]}.$$

III. ANALYSIS OF THE FLOW FIELD AND DISCUSSION

A. General features in the case of a stationary outer cylinder

When acceleration terms are absent, the limiting behavior of the flow field is the solid-body rotation: $\Omega \leqslant |\Omega_2 - \Omega_1|$. In other words, the local angular velocity cannot exceed the angular velocity of the driving cylinder. This is a property of both models, in the form $u^*_{\theta_1} - \chi u^*_{\theta_2} \geqslant 0$. Such a constraint can also be derived from (3) by noting that the value of b must be non-negative in order to achieve a physical solution. Furthermore, due to the positive sign of the second derivative of the velocity profile, which is apparent from Eq. (8), the maximum velocity in the flow occurs at either the inner or outer cylinder. However, a locally inverted velocity profile may appear, and in some cases a fully inverted velocity profile can be predicted. The existence of an inverted velocity can best be illustrated via Fig. 1, where a velocity polar is introduced. The velocity polar is a plot on the hodograph plane $(u^*_{\theta_1}, u^*_{\theta_2})$ which is defined as the locus of all possible $u^*_{\theta_1}(\alpha)$ and $u^*_{\theta_2}(\alpha)$ for a given χ. The velocities on the cylinders fall within three limits: solid-body rotation, $\chi \to 1$, and $\chi \to 0$. The trajectory of the velocities for a given χ in this plot is obtained from Eq. (A17) and (A18) of the Langmuir model and from Eq. (B14) and (B15) of the Maxwell model. The lines defined by (A17) and (B14) represent the shear stress in the hodograph plane, while the lines defined by (A18) and (B15) represent the relationship of velocities $u^*_{\theta_1}$, $u^*_{\theta_2}$ for a given χ. The exact values of the velocities are determined by the common point of these two lines. It can be easily seen in this plot that, depending on the value of α, noninverted, partially inverted, and fully inverted velocity profiles can appear. The Langmuir and Maxwell models yield almost the same predictions, in qualitative agreement with the DSMC data of Aoki, Yoshida, Nakanishi, and Garcia,[16] despite the two models being developed from totally independent considerations of the gas-surface molecular interaction. The flow conditions considered by Aoki, Yoshida, Nakanishi, and Garcia[16] in their recent DSMC calculation for hard-sphere molecules were

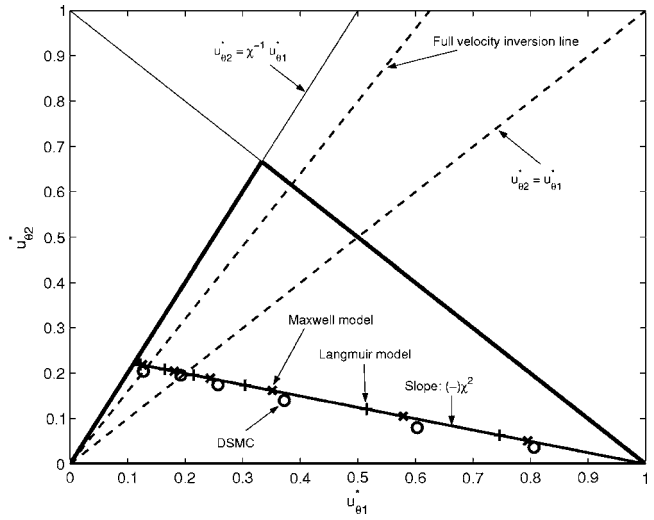

FIG. 1. A velocity polar on the hodograph plane (for stationary outer cylinder). The full velocity-inversion line is defined as $u^*_{\theta_2} = (1+\chi^2)/(2\chi)u^*_{\theta_1}$. The value of α decreases with decreasing $u^*_{\theta_1}$ and six values (0.714, 0.455, 0.217, 0.116, 0.0602, and 0.0124) are considered in this plot. The assumptions of $\omega = \omega_M$, $\chi = 0.5$, and Kn = 0.1 are applied to the theoretical models and the DSMC result. The (+), (×), and (○) symbols represent the Langmuir, Maxwell, and DSMC results, respectively.

$$M = 0.548, \quad \mathrm{Kn} = \lambda/(20\lambda - 10\lambda) = 0.1,$$

$$\chi = 10\lambda/(20\lambda) = 0.5.$$

Qualitative agreement between the two models can also be seen in Fig. 2, where the topology of the velocity is described in the three-dimensional space $(u^*_{\theta_1}, u^*_{\theta_2}, 1-\alpha)$. The topology is represented by a straight line in the Langmuir model and a curve in the Maxwell model. A similar observation can be made in Fig. 3, where the value of $(u^*_{\theta_1} - \chi u^*_{\theta_2})$—equivalently the stresses, which is evident in Eq. (3)—is plotted against α. It can be seen that the drag coefficients relative to no-slip values are proportional to the degree of nonequilibrium represented by α, that is, $(1+4\omega\mathrm{Kn})^{-1}$. This property is qualitatively similar to the result for cylindrical Couette flow of a rarefied gas produced via the linearized Boltzmann equation.[28]

In Fig. 4 the critical values of α for full velocity inversion are plotted against the radius ratio χ. Such values are obtained in the Langmuir model by noting that the first inequality in (9) is always satisfied for the relations (20) and (21) and the second inequality reduces to

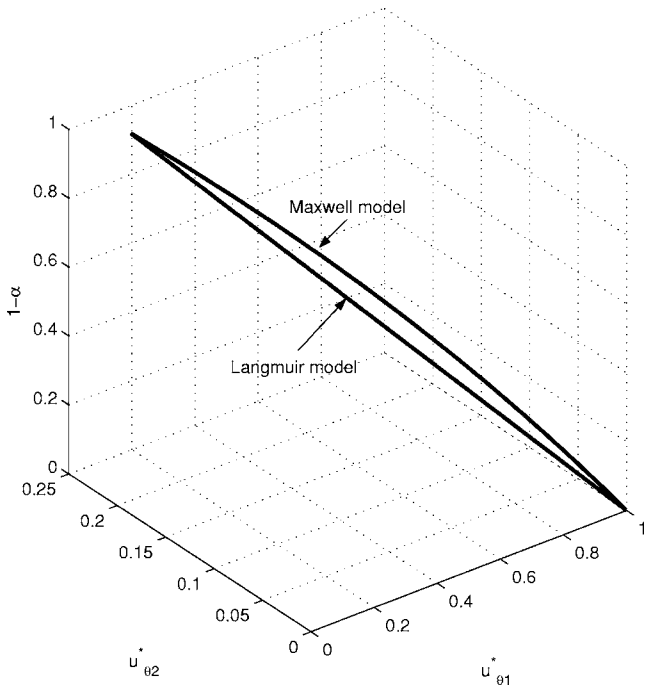

FIG. 2. Topology of the velocity as described by the three-dimensional space $(u^*_{\theta_1}, u^*_{\theta_2}, 1-\alpha)$ (for stationary outer cylinder, $\omega=\omega_M$, $\chi=0.5$).

$$\alpha < \alpha_{\text{crit}} \quad \text{where} \quad \alpha_{\text{crit}} \equiv \frac{\chi^3(1-\chi)}{2\chi^2-\chi+1}.$$

Full velocity inversion occurs, therefore, whenever the value of α is smaller than α_{crit}. In the case of the Maxwell model, the critical value $\alpha_{M_{\text{crit}}}$ becomes

$$\alpha_{M_{\text{crit}}} \equiv \frac{\chi^2(1-\chi)}{2+3\chi^2-\chi^3}.$$

Interestingly, the critical values of both models coincide at the golden ratio[29] $\chi=2^{-1}(3-5^{1/2}) \doteq 0.382$. In fact, if we assume the following relation between the Langmuir and Maxwell models,

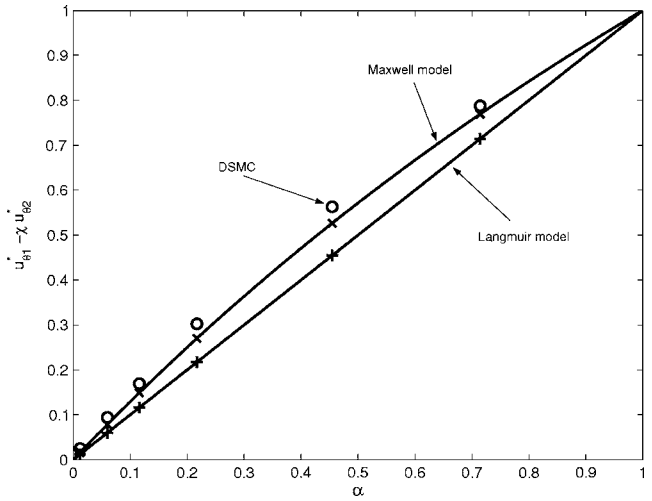

FIG. 3. Trajectory of the shear stress on the cylinder plotted by the degree of nonequilibrium α (for stationary outer cylinder). Other conditions are the same as in Fig. 1.

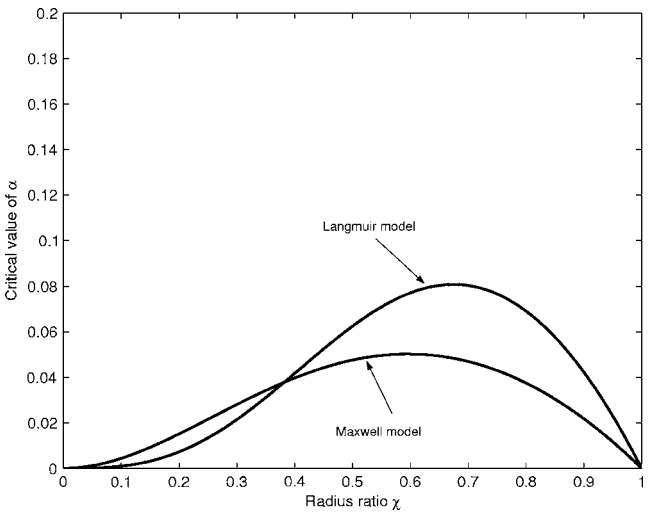

FIG. 4. Range of α values for full velocity inversion. The value of α_{crit} in the Langmuir model has a maximum of 8.085×10^{-2} at $\chi=0.6746$, while the value of $\alpha_{M_{\text{crit}}}$ in the Maxwell model has a maximum of 5.028×10^{-2} at $\chi=0.5961$.

$$\omega_M = f\omega, \quad \text{equivalently} \quad \alpha_M = \frac{\alpha}{\alpha + f(1-\alpha)},$$

where

$$f \equiv \frac{2\chi}{1-\chi+\chi^2},$$

then the two models yield exactly the same solutions, including the velocity profile.

On the other hand, from (22) it can be seen that the family of velocity profiles all pass through a common point irrespective of the value of α:

$$r^* = \frac{(1-\chi+\chi^2)^{1/2}}{\chi},$$

which is the reference radius $\bar{R}^*$ given in (A20). The existence of a common point was first identified for the Maxwell model by Yuhong, Barber, and Emerson,[18] and the present study confirms it. In fact, both models share exactly the same common point, in spite of the difference in the velocity profiles.

B. Effect of different wall conditions

The surfaces of the cylinders can have different accommodation coefficients, depending on the type of material used and the surface treatment. In the Langmuir model, such effects are incorporated by the coefficient ω in (14). Its value is in the range of $0<\omega<\infty$, if repulsion in addition to attraction is allowed in defining the potential energy D_e. On the other hand, in the Maxwell model it is represented by the coefficient $\omega_M(1<\omega_M<\infty)$ in (16). The effect of different coefficients on the velocities can be analyzed from (A8) together with (A9) and from (B5) together with (B6). In the Langmuir model, we find

$$\frac{\alpha_1}{D_L} = \frac{1}{1 - q(1 - \alpha_2/\alpha_1)},$$

thus

$$\frac{\alpha_1}{D_L} < 1 \quad \text{when} \quad \alpha_1 < \alpha_2 \quad \text{and} \quad \frac{\alpha_1}{D_L} > 1 \quad \text{when} \quad \alpha_1 > \alpha_2.$$

This means that when $\alpha_1 > \alpha_2$ the velocity trajectories move upward in the hodograph plane, since the slope m_L remains the same. In addition, the slope of the stress curve defined by (A4) increases, giving rise to an inverted velocity profile. However, when $\alpha_1 < \alpha_2$ the velocity trajectories move downward in the hodograph plane and the slope of the stress curve decreases, causing no inverted velocity profile. From this reasoning, it can be concluded that the small value of α_2 plays a critical role in whether velocity inversion occurs or not. In fact, it can be proved from Eqs. (A6), (A7), and (9) that if $\alpha_2 < \alpha_{\text{crit}}$ the solution is always a fully inverted velocity profile, irrespective of the value of α_1. Equivalently, no inverted velocity profile can be found when the value of α_2 is close to unity.

A similar description is possible for the Maxwell model. From (B5) and (B6), the velocity trajectories always meet the $u^*_{\theta_2}=0$ axis at the point $u^*_{\theta_1}=1$, and its slope will satisfy the following relations:

$$m_M \sim \frac{\alpha_{M_1}}{(1 - \alpha_{M_1})} \quad \text{for a given} \quad \alpha_{M_2},$$

$$m_M \downarrow \quad \text{when} \quad \alpha_{M_1} < \alpha_{M_2} \quad \text{and} \quad m_M \uparrow \quad \text{when} \quad \alpha_{M_1} > \alpha_{M_2}.$$

Therefore, when $\alpha_{M_1} > \alpha_{M_2}$ the slope of the velocity trajectories increases in the hodograph plane, causing an increase in slip at the stationary outer cylinder. Similar explanations to those above are possible through the examination of Eqs. (B7) and (B8).

C. The case of a stationary inner cylinder

For the case of a stationary inner cylinder, the velocities in the hodograph plane are determined by the following equations in the Langmuir model ($m_L=\chi^2$):

$$u^*_{\theta_2} - \chi^{-1} u^*_{\theta_1} = \alpha,$$

$$u^*_{\theta_2} = -m_L u^*_{\theta_1} + 1,$$

and in the Maxwell model ($m_M=\chi^2$) by

$$u^*_{\theta_2} - \chi^{-1} u^*_{\theta_1} = \frac{2\alpha_M \chi}{2\alpha_M \chi + (1 - \alpha_M)(1 - \chi + \chi^2)},$$

$$u^*_{\theta_2} = -m_M u^*_{\theta_1} + 1.$$

Here, the velocity was expressed in terms of the quantity $(R_2\Omega_2)$. Similar to the previous case of a stationary outer cylinder, the velocities are defined within three limits: solid-body rotation, $\chi \to 1$, and $\chi \to 0$ (or $u^*_{\theta_2}=1$), which are illustrated by the thick solid lines in Fig. 5. However, no inverted velocity profile will appear since the solid-body limit enforces $u^*_{\theta_2} \geqslant u^*_{\theta_1}$ (the equality occurs only when $\chi \to 1$ and $\alpha \to 0$).

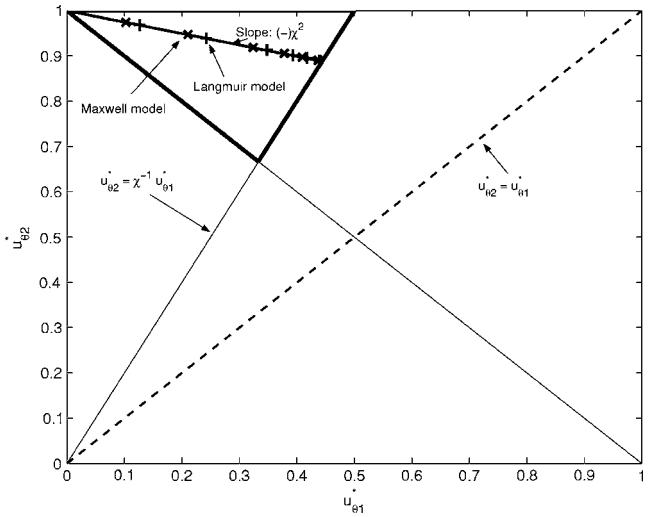

FIG. 5. A velocity polar on the hodograph plane (for stationary inner cylinder). The value of α decreases with decreasing $u^*_{\theta_2}$ in this plot. Other conditions are the same as in Fig. 1, except that DSMC results are not available for the present case.

D. Discussion

At this stage it is instructive to examine the velocity-inversion phenomenon from a physical point of view. In the continuum limit the angular momentum attained from the rotating inner cylinder is continuously transferred to the outer region through viscous friction (molecular collisions) until it vanishes at the stationary outer cylinder. However, when the fraction reaching the thermal equilibrium α decreases through either large slip coefficients ω or non-negligible Knudsen numbers, the velocity slip at the wall causes the angular momentum near the outer cylinder to increase while the angular momentum near the inner cylinder decreases. In particular, the braking effect of the outer cylinder is reduced by the velocity slip and as a result the flow in the outer region can gain angular momentum continuously. As α decreases further, then the inversion of the angular momentum in the radial direction will appear, followed by the inversion of the velocity profile. Finally, solid-body rotation with a constant angular rate will form in the limit of α tending to zero.

There are elements in the two slip models related to the effect of curvature that produce this velocity inversion. In the case of the Langmuir model, the quantity used to determine the momentum slip in a concentric cylindrical geometry should be based upon the angular velocity Ω or u_θ/r, not the velocity u_θ itself [see Eq. (19)]. For the Maxwell model, a component of the shear stress associated with the curvature, $(-)\mu u_\theta/r$, is responsible for the inverted velocity profile. Once these aspects are incorporated, both models are capable of capturing the velocity-inversion phenomena. Qualitatively, the results are the same even when the reference radius ratio $\bar{R}$ in the Langmuir model is defined differently from the geometric average (A20) if a consistency condition

is met: $\bar{R}\rightarrow$ an average of R_1 and R_2 for $R_1 \approx R_2$ and $\bar{R} \rightarrow R_2$ for $R_1 \ll R_2$. In fact, it can be shown that only a minor change in the slope (A9) of the velocity curve defined as (A8) occurs on introducing a different average, and thus the qualitative results of the velocity inversion are unchanged.

When the Knudsen number is sufficiently large, the present prediction on the basis of linear theory and slip corrections may not describe the real physics of rotating cylindrical Couette flow. A recent DSMC calculation[16] has indicated that the velocity profile inversion may not appear at high Kn. This could be because only a small fraction of the angular momentum gained from the rotating inner cylinder will be transferred to the outer region when molecular collisions are so rare. In other words, the gas velocity in the outer region will remain low due to this lack of angular momentum transfer, while the gas velocity near the rotating inner cylinder remains relatively high. This effect at high Kn is the subject of future investigation.

In connection with this molecular explanation, it is possible to examine the implications of our present formulation for high Knudsen number flows from a macroscopic point of view. The degree of nonequilibrium considered in the present study, and in previous work by Aoki, Yoshida, Nakanishi, and Garcia[16] and Tibbs, Baras, and Garcia,[15] can be approximated by

$$N_\delta \sim \mathrm{Kn}\, M = 0.055.$$

A different estimate is also possible through a direct calculation of the ratio of the stress to the pressure. If we assume $\lambda = 6.25 \times 10^{-8}$ m and $\Omega_1 = 2.82 \times 10^8$ rad/s, then we can estimate the shear stress on the stationary outer cylinder—which plays a critical role in the inverted velocity profile—by the Langmuir model. The shear stress is about 2.8% of atmospheric pressure

$$\left|[\tau_{r\theta}]_{r=R_2}\right| = \mu\Omega_1 \frac{2\alpha\chi^2}{1-\chi^2} \doteqdot 2.82 \times 10^3 \ \mathrm{N/m^2},$$

where a viscosity of 2.1×10^{-5} N s/m^2 is assumed. An estimate of the non-Newtonian coupling effect[24] from the constitutive relations of Grad[30] and Eu,[4] Myong,[31] and Khayat and Eu[32] yields

$$\left|[\tau_{\theta\theta} - \tau_{rr}]_{r=R_2}\right| = p\left[\frac{6(\tau_{r\theta}/p)^2}{3 + 2(\tau_{r\theta}/p)^2}\right] \doteqdot 1.57 \times 10^2 \ \mathrm{N/m^2},$$

meaning that the normal stress generated by the shear velocity is only a small fraction of the shear stress (in this case 5.6%). Thus ignoring normal stress effects can be justified in the present study. However, for flows with higher Knudsen numbers or Mach numbers,[32–35,16] for example, Kn=1.0 or beyond, there will be significant differences due to non-Newtonian coupling, in particular, the normal stress may become non-negligible. The normal stress may act to oppose the reduction of the braking effect at the stationary outer cylinder due to the velocity slip associated with the gas-surface molecular interaction, which could explain the disappearance of velocity inversion.

IV. CONCLUDING REMARKS

In this paper we have shown that the velocity-inversion phenomenon in microscale cylindrical Couette flow can be described by the Langmuir slip model based on the concept of gaseous adsorption onto solids. Nonequilibrium effects on the flow topology can be more clearly illustrated by introducing a velocity polar on the hodograph plane. For mathematical simplicity, the present study has been limited to the investigation of velocity slip phenomena. Extension to nonisothermal cases involving temperature jumps at the solid surfaces, and the use of nonlinear high-order constitutive relations to model the nonequilibrium bulk flow, will be the subject of future work.

ACKNOWLEDGMENTS

We thank the Engineering and Physical Sciences Research Council (EPSRC) of the United Kingdom for its financial support of this research under Grant No. GR/S77196/01. One of the authors (R.S.M.) especially thanks the Department of Mechanical Engineering, University of Strathclyde, UK, for the hospitality extended to him during his stay. One of the authors (R.S.M.) also acknowledges partial support provided by the Korea Research Foundation Grant No. KRF-2003-013-D00018.

APPENDIX A: SOLUTIONS OF THE LANGMUIR SLIP MODEL

The velocity relation (2) and boundary conditions (17) and (18) in the Langmuir model can be written in dimensionless form as

$$u_\theta^*(r^*) = \frac{1}{D}\left[(\chi u_{\theta_1}^* - u_{\theta_2}^*)r^* + (u_{\theta_2}^* - u_{\theta_1}^*\chi^{-1})r^{*-1}\right], \tag{A1}$$

$$u_{\theta_1}^* = \alpha_1 + (1-\alpha_1)u_\theta^*(\bar{R}^*)\frac{1}{\bar{R}^*}, \tag{A2}$$

$$u_{\theta_2}^* = \chi^{-1}\left[\alpha_2\bar{\Omega} + (1-\alpha_2)u_\theta^*(\bar{R}^*)\frac{1}{\bar{R}^*}\right]. \tag{A3}$$

It can be seen that there exists a relationship between $u_{\theta_1}^*$ and $u_{\theta_2}^*$,

$$(1-\alpha_2)u_{\theta_1}^* - \chi(1-\alpha_1)u_{\theta_2}^* = \alpha_1(1-\alpha_2) - \bar{\Omega}\alpha_2(1-\alpha_1). \tag{A4}$$

For very small values of α_1, α_2, this approaches the following limit:

$$u_{\theta_1}^* \approx \chi u_{\theta_2}^*. \tag{A5}$$

By combining with the velocity Eq. (A1), we can determine the velocities on the cylinders in terms of χ, α_1, α_2, $\bar{\Omega}$, and $\bar{R}^*$ from relations (A2) and (A3). They take the following form:

$$u_{\theta_1}^* = \{\alpha_1[1-(1-\alpha_2)q] + \bar{\Omega}\alpha_2(1-\alpha_1)q\}/D_L, \tag{A6}$$

$$u_{\theta_2}^* = \{\alpha_1(1-\alpha_2)p + \bar{\Omega}\alpha_2[\chi^{-1} - (1-\alpha_1)p]\}/D_L, \tag{A7}$$

where

$$p = \frac{1-(\chi\bar{R}^*)^{-2}}{D}, \quad q = 1-\chi p = -\frac{\chi^{-1}(1-\bar{R}^{*-2})}{D},$$

$$D_L = 1-[(1-\alpha_1)\chi p + (1-\alpha_2)q].$$

In addition, there exists a relationship between $u_{\theta_1}^*$ and $u_{\theta_2}^*$,

$$u_{\theta_2}^* - \chi^{-1}\bar{\Omega}(\alpha_2/D_L) = -m_L[u_{\theta_1}^* - (\alpha_1/D_L)], \tag{A8}$$

where, if $\bar{R}^*$ is given as a function of the ratio χ, the slope m_L becomes dependent on the ratio χ only,

$$m_L\left(\equiv\frac{p}{q}\right) = -\frac{\chi\bar{R}^{*2}-\chi^{-1}}{\bar{R}^{*2}-1}, \tag{A9}$$

where

$$0 \leqslant m_L \leqslant 1.$$

As a result, the velocities can be expressed in terms of χ, α_1, α_2, and $\bar{\Omega}$. Finally, by using the general relation for the shear stress (3), we can obtain the following relation in the present slip model:

$$\frac{\tau_{r\theta}}{\mu\Omega_1} = \frac{2}{D}(\chi^{-1}u_{\theta_1}^* - u_{\theta_2}^*)r^{*-2} = \frac{2}{D}\frac{\alpha_1\alpha_2(1-\bar{\Omega})}{D_L\chi}r^{*-2}. \tag{A10}$$

Thus the following relation is always satisfied:

$$\left[\frac{\tau_{r\theta}}{\mu\Omega_1}\right]_{r^*=1} = \chi^{-2}\left[\frac{\tau_{r\theta}}{\mu\Omega_1}\right]_{r^*=1/\chi}.$$

For simplicity, we first consider the case $\alpha_1=\alpha_2(=\alpha)$. Then $D_L=\alpha$ and thereby the solutions reduce to

$$u_{\theta_1}^* = 1-(1-\bar{\Omega})(1-\alpha)q, \tag{A11}$$

$$u_{\theta_2}^* = \chi^{-1}\bar{\Omega} + (1-\bar{\Omega})(1-\alpha)p, \tag{A12}$$

which can also be derived from

$$u_{\theta_1}^* - \chi u_{\theta_2}^* = \alpha(1-\bar{\Omega}), \tag{A13}$$

$$u_{\theta_2}^* - \chi^{-1}\bar{\Omega} = -m_L(u_{\theta_1}^* - 1). \tag{A14}$$

They can be further simplified when $\Omega_2=0$,

$$u_{\theta_1}^* = 1-(1-\alpha)q, \tag{A15}$$

$$u_{\theta_2}^* = (1-\alpha)p, \tag{A16}$$

and

$$u_{\theta_1}^* - \chi u_{\theta_2}^* = \alpha, \tag{A17}$$

$$u_{\theta_2}^* = -m_L(u_{\theta_1}^* - 1). \tag{A18}$$

Now the detailed form of the reference position must be specified in order to determine the velocity profile. In general, it may be written as

$$\bar{R} = R_1 + (R_2-R_1)f(\kappa_1,\kappa_2),$$

or, in the case of the geometric average,

$$\bar{R}^2 = R_2[R_1 + (R_2-R_1)f(\kappa_1,\kappa_2)],$$

where κ represents the curvature of the wall, which in polar coordinates becomes

$$\kappa = \frac{r^2+2r_\theta^2-rr_{\theta\theta}}{(r^2+r_\theta^2)^{3/2}}.$$

In this paper we propose the following form of the function f in the geometric average, which is the simplest form among the candidates

$$f(\kappa_1,\kappa_2) = 1-\frac{\kappa_2}{\kappa_1}.$$

By noting that $\kappa=1/R$ in concentric cylinders with a constant radius, we can obtain the following reference radius:

$$\bar{R}^2 = R_2\left[R_1 + (R_2-R_1)\left(1-\frac{R_1}{R_2}\right)\right], \tag{A19}$$

where $\bar{R}\to\sqrt{R_1R_2}$ for $\kappa_1\approx\kappa_2$ and $\bar{R}\to R_2$ for $\kappa_1\gg\kappa_2$. The reference radius can then be expressed in dimensionless form

$$\bar{R}^{*2} = \frac{1-\chi+\chi^2}{\chi^2}. \tag{A20}$$

Finally, the solutions can be obtained by using the following coefficients:

$$p = \frac{\chi^2}{1+\chi^3}, \quad q = \frac{1}{1+\chi^3}, \quad m_L = \chi^2. \tag{A21}$$

APPENDIX B: SOLUTIONS OF THE MAXWELL SLIP MODEL

The velocity relation (2) and boundary conditions (24) and (25) in the Maxwell model can be written in dimensionless form as

$$u_{\theta_1}^* = 1-\frac{(1-\alpha_{M_1})}{\alpha_{M_1}}\frac{(\chi^{-1}u_{\theta_1}^* - u_{\theta_2}^*)}{2(1+\chi)}, \tag{B1}$$

$$u_{\theta_2}^* = \chi^{-1}\bar{\Omega} + \frac{(1-\alpha_{M_2})}{\alpha_{M_2}}\frac{(\chi^{-1}u_{\theta_1}^* - u_{\theta_2}^*)}{2(1+\chi)}\chi^2. \tag{B2}$$

Like the Langmuir model, there exists an upper limit for very small values of α_{M_1}, α_{M_2}:

$$u_{\theta_1}^* \approx \chi u_{\theta_2}^*. \tag{B3}$$

In addition, there are two relationships between $u_{\theta_1}^*$ and $u_{\theta_2}^*$,

$$u_{\theta_1}^* - \chi u_{\theta_2}^* = \frac{2\alpha_{M_1}\alpha_{M_2}(1+\chi)(1-\bar{\Omega})}{D_M}, \tag{B4}$$

where

$$D_M = 2(1+\chi)\alpha_{M_1}\alpha_{M_2} + \chi^{-1}\alpha_{M_2}(1-\alpha_{M_1}) + \chi^2\alpha_{M_1}(1-\alpha_{M_2}),$$

and

$$u_{\theta_2}^* - \chi^{-1}\bar{\Omega} = -m_M(u_{\theta_1}^* - 1), \tag{B5}$$

where

$$m_M = \frac{\alpha_{M_1}(1-\alpha_{M_2})}{\alpha_{M_2}(1-\alpha_{M_1})}\chi^2. \tag{B6}$$

We can then determine the velocities in terms of χ, α_1, α_2, and $\bar{\Omega}$ from the relations (B1) and (B2) or (B4) and (B5),

$$u_{\theta_1}^* = 1 - (1-\bar{\Omega})\chi^{-1}\alpha_{M_2}(1-\alpha_{M_1})/D_M, \tag{B7}$$

$$u_{\theta_2}^* = \chi^{-1}\{1 - (1-\bar{\Omega})\alpha_{M_2}[2(1+\chi)\alpha_{M_1} + \chi^{-1}(1-\alpha_{M_1})]/D_M\}. \tag{B8}$$

We can also derive the following shear stress relation from (3)

$$\frac{\tau_{r\theta}}{\mu\Omega_1} = \frac{4\alpha_{M_1}\alpha_{M_2}(1+\chi^{-1})(1-\bar{\Omega})}{DD_M}r^{*-2}. \tag{B9}$$

When $\alpha_{M_1}=\alpha_{M_2}(=\alpha_M)$, the solutions reduce to

$$u_{\theta_1}^* = 1 - (1-\bar{\Omega})\chi^{-1}\alpha_M(1-\alpha_M)/D_M, \tag{B10}$$

$$u_{\theta_2}^* = \chi^{-1}\{1 - (1-\bar{\Omega})\alpha_M[2(1+\chi)\alpha_M + \chi^{-1}(1-\alpha_M)]/D_M\}, \tag{B11}$$

where

$$D_M = 2\alpha_M^2(1+\chi) + \alpha_M(1-\alpha_M)(\chi^{-1}+\chi^2).$$

They can be further simplified when $\Omega_2=0$,

$$u_{\theta_1}^* = \frac{2\alpha_M\chi(1+\chi) + (1-\alpha_M)\chi^3}{2\alpha_M\chi(1+\chi) + (1-\alpha_M)(1+\chi^3)}, \tag{B12}$$

$$u_{\theta_2}^* = \frac{(1-\alpha_M)\chi^2}{2\alpha_M\chi(1+\chi) + (1-\alpha_M)(1+\chi^3)}, \tag{B13}$$

which satisfy the equations (B4) and (B5)

$$u_{\theta_1}^* - \chi u_{\theta_2}^* = \frac{2\alpha_M\chi}{2\alpha_M\chi + (1-\alpha_M)(1-\chi+\chi^2)}, \tag{B14}$$

$$u_{\theta_2}^* = -\chi^2(u_{\theta_1}^* - 1). \tag{B15}$$

[1] J. M. Reese, M. A. Gallis, and D. A. Lockerby, "New directions in fluid dynamics: Non-equilibrium aerodynamic and microsystem flows," Philos. Trans. R. Soc. London, Ser. A **361**, 2967 (2003).

[2] G. E. Karniadakis and A. Beskok, *Micro Flows: Fundamentals and Simulation* (Springer, New York, 2002).

[3] S. Chapman and T. G. Cowling *The Mathematical Theory of Nonuniform Gases*, 3rd ed. (Cambridge University Press, Cambridge, 1970).

[4] B. C. Eu, *Kinetic Theory and Irreversible Thermodynamics* (Wiley, New York, 1992).

[5] B. C. Eu, *Generalized Thermodynamics: The Thermodynamics of Irreversible Processes and Generalized Hydrodynamics* (Kluwer, Dordrecht, 2002).

[6] T. I. Gombosi, *Gaskinetic Theory* (Cambridge University Press, Cambridge, 2002).

[7] C. Cercignani, *Rarefied Gas Dynamics: From Basic Concepts to Actual Calculations* (Cambridge University Press, Cambridge, 2000).

[8] J. C. Maxwell, "On stresses in rarefied gases arising from inequalities of temperature," Philos. Trans. R. Soc. London **170**, 231 (1879).

[9] J. C. Shih, C. M. Ho, J. Liu, and Y. C. Tai, "Monatomic and polyatomic gas flow through uniform microchannels," ASME MEMS, DSC **59**, 197 (1996).

[10] E. B. Arkilic, M. A. Schmidt, and K. S. Breuer, "Gaseous slip flow in long microchannels," J. Microelectromech. Syst. **6**, 167 (1997).

[11] R. Schamberg, "The fundamental differential equations and the boundary conditions for high speed slip flow," Ph.D. thesis, California Institute of Technology, 1947.

[12] T. C. Lin, and R. E. Street, "Effect of variable viscosity and thermal conductivity on high-speed slip flow between concentric cylinders," NACA Report No. 1175, 1954 (unpublished).

[13] K. Nanbu, "Analysis of cylindrical Couette flows by use of the direct simulation method," Phys. Fluids **27**, 2632 (1984).

[14] D. Einzel, P. Panzer, and M. Liu, "Boundary condition for fluid flow: Curved or rough surfaces," Phys. Rev. Lett. **64**, 2269 (1990).

[15] K. W. Tibbs, F. Baras, and A. L. Garcia, "Anomalous flow profile due to the curvature effect on slip length," Phys. Rev. E **56**, 2282 (1997).

[16] K. Aoki, H. Yoshida, T. Nakanishi, and A. L. Garcia, "Inverted velocity profile in the cylindrical Couette flow of a rarefied gas," Phys. Rev. E **68**, 016302 (2003).

[17] D. A. Lockerby, J. M. Reese, D. R. Emerson, and R. W. Barber, "Velocity boundary condition at solid walls in rarefied gas calculations," Phys. Rev. E **70**, 017303 (2004).

[18] S. Yuhong, R. W. Barber, and D. R. Emerson, "Inverted velocity profiles in rarefied cylindrical Couette gas flow and the impact of the accommodation coefficient," Phys. Fluids **17**, 047102 (2005).

[19] D. J. Alofs and G. S. Springer, "Cylindrical Couette flow experiments in the transition regime," Phys. Fluids **14**, 298 (1971).

[20] G. A. Bird, *Molecular Gas Dynamics and the Direct Simulation of Gas Flows* (Clarendon, Oxford, England, 1994).

[21] B. C. Eu, R. E. Khayat, G. D. Billing, and C. Nyeland, "Nonlinear transport coefficients and plane Couette flow of a viscous, heat-conducting gas between two plates at different temperatures," Can. J. Phys. **65**, 1090 (1987).

[22] D. K. Bhattacharya and B. C. Eu, "Nonlinear transport processes and fluid dynamics: Effects of thermoviscous coupling and nonlinear transport coefficients on plane Couette flow of Lennard-Jones fluids," Phys. Rev. A **35**, 821 (1987).

[23] R. S. Myong, "Velocity-slip effect in low-speed microscale gas flows," AIAA Paper No. 2001-3076, 2001 (unpublished).

[24] R. S. Myong, "Gaseous slip models based on the Langmuir adsorption isotherm," Phys. Fluids **16**, 104 (2004).

[25] R. S. Myong, "A generalized hydrodynamic computational model for rarefied and microscale diatomic gas flows," J. Comput. Phys. **195**, 655 (2004).

[26] I. Langmuir, "Surface chemistry," Chem. Rev. (Washington, D.C.) **13**, 147 (1933).

[27] A. W. Adamson, *Physical Chemistry of Surfaces* (Wiley, New York, 1982).

[28] C. Cercignani and F. Sernagiotto, "Cylindrical Couette flow of a rarefied gas," Phys. Fluids **10**, 1200 (1967).

[29] M. Livio, *The Golden Ratio: The Story of Phi, the World's Most Astonishing Number* (Broadway Books, New York, 2002).

[30] H. Grad, "On the kinetic theory of rarefied gases," Commun. Pure Appl. Math. **2**, 331 (1949).

[31] R. S. Myong, "Thermodynamically consistent hydrodynamic computational models for high-Knudsen-number gas flows," Phys. Fluids **11**, 2788 (1999).

[32]R. E. Khayat and B. C. Eu, "Generalized hydrodynamics, normal-stress effects, and velocity slips in the cylindrical Couette flow of Lennard-Jones fluids," Phys. Rev. A **39**, 728 (1989).

[33]L. M. de Socio and L. Marino, "Simulation and modelling of flows between rotating cylinders. Influence of Knudsen number," Math. Models Meth. Appl. Sci. **10**, 73 (2000).

[34]W. Marques, Jr. and G. M. Kremer, "Couette flow from a thirteen field theory with slip and jump boundary conditions," Continuum Mech. Thermodyn. **13**, 207 (2001).

[35]L. M. G. Cumin, G. M. Kremer, and F. Sharipov, "The influence of slip and jump boundary conditions on the cylindrical Couette flow," Math. Models Meth. Appl. Sci. **12**, 445 (2002).